

## THE FIRST YEAR OF MARK-J AT PETRA

D.P. Barber, U. Becker\*, H. Benda, A. Boehm, J.G. Branson, J. Bron, D. Buikman, J. Burger, C.C. Chang, H.S. Chen, M. Chen, C.P. Cheng, Y.S. Chu, R. Clare, P. Duinker, G.Y. Fang, H. Fesefeldt, D. Fong, M. Fukushima, J.C. Guo, A. Hariri, G. Herten, M.C.Ho, H.K. Hsu, T.T. Hsu, R.W. Kadel, W. Krenz, J. Li, Q.Z. Li, M. Lu, D. Luckey, D.A. Ma, C.M. Ma, G.G.G. Massaro, T. Matsuda, H. Newman, J. Paradiso, F.P. Poschmann, J.P. Revol, M. Rohde, H. Rykaczewski, K. Sinram, H.W. Tang, L.G. Tang, Samuel C.C. Ting, K.L. Tung, F. Vannucci\*, X.R. Wang, P.S. Wei, M. White, G.H. Wu, T.W. Wu, J.P. Xi, P.C. Yang, X.H. Yu, N.L. Zhang and R.Y. Zhu.

III. Physikalisches Institut Technische Hochschule, Aachen, West Germany

Deutsches Elektronen-Synchrotron (DESY), Hamburg, West Germany

Laboratory for Nuclear Science, Massachusetts Institute of Technology, Cambridge, Massachusetts, U.S.A.

Nationaal Instituut voor Kernfysika en Hoge-Energiefysica (NIKHEF), Sectie H, Amsterdam, The Netherlands, and

Institute of High Energy Physics, Chinese Academy of Science, Peking, People's Republic of China.

\*currently at CERN, Geneva, Switzerland

Presented by Harvey Newman

### Abstract

We report on the experimental results by the MARK-J collaboration at PETRA on measurements of  $R$ , on tests of quantum electrodynamics and charged lepton universality and the discovery of three jet events due to gluon emission.

The MARK-J detector is shown in Figs. 1, 2, 3 and 4. It is a detector designed to measure and distinguish hadrons, electrons, neutral particles, and muons. It covers a solid angle of  $\phi = 2\pi$  and  $\theta = 9^\circ$  to  $171^\circ$  ( $\theta$  is the polar and  $\phi$  is the azimuthal angle). The detector is symmetrical in both  $\phi$  and  $\theta$  directions. The physics objectives of this detector are:

- (1) to measure the interference effects between weak and electromagnetic interactions by studying the charge asymmetry in the reaction  $e^+e^- \rightarrow \mu^+\mu^-$  with an accuracy of 1%,
- (2) to measure the total hadron production cross section,
- (3) to study various quantum electrodynamic processes,
- (4) to measure  $\mu e$  and  $\mu$  hadron events and to study asymmetries associated with these events which can come from weak interaction effects, and
- (5) to search for new quarks and heavy leptons.

As shown in Fig. 1, the particles leaving the interaction region pass through a ring of 32 lucite Cerenkov counters, L. These counters are used to distinguish charged particles from neutrals and are insensitive to synchrotron radiation and they cover a

range of  $\theta = 9^\circ$  to  $171^\circ$ . The twenty A counters have one phototube at each end, are constructed from three radiation lengths of lead sandwiched with 5 mm of scintillators, and cover an angular region of  $\theta = 12^\circ$  to  $168^\circ$ . The 24 B counters are constructed identically to the A counters and cover an angular region of  $\theta = 16^\circ$  to  $164^\circ$ . The counters A and B enable us to locate shower maxima in various  $\theta$  and  $\phi$  directions. Surrounding these are sixteen C shower counters consisting of twelve layers (twelve radiation lengths) of lead-scintillator sandwich also with one tube at each end. The drift chambers S and T have twelve planes and U and V have ten planes. They are used to sample hadron showers and measure the original muon tracks with a spatial resolution  $\approx 400 \mu\text{m}^{1),2)}$ . The hadron calorimeter K consists of 192 counters sandwiched with magnetized iron to measure hadron showers. The magnetic field in the iron is toroidal and its value is 17 kG. Finally, in the outermost layer, we have the P and R drift chambers which are used to measure muon exit angles and thus momenta. These chambers have ten to sixteen planes each. The Q drift chambers adjacent to the D counters have two planes. They measure the muon tracks in the bending

plane. The 32 D and 16 E hodoscopes have dimensions of 30cm x 450cm x 1cm and 80cm x 450cm x 1cm, respectively, and are used to trigger on single and multiple muon events and to reject cosmic rays and beam spray. Fig. 3 is a photograph of the MARK-J detector in its final position in the beam. The study of weak-electromagnetic interference involves a very sensitive measurement of asymmetries. In order to nullify any effects due to inherent asymmetries of the detector in the  $\phi$  and  $\theta$  directions, the supporting structure was made so that the detector can rotate  $\pm 90^\circ$  in  $\phi$  and  $180^\circ$  in  $\theta$ . Fig. 4 shows the detector in a rotated position in one of the stages of assembly. The total weight of the detector is about 500 tons and by survey measurements it was found that the axis of the  $\phi$  rotation is reproducible to 200 microns.

One quarter of the complete assembly was tested and calibrated at a muon, electron and pion beam at CERN. The gain of all the counters was adjusted according to the test results.

The luminosity monitor consists of two arrays of twenty eight lead glass counters<sup>3)</sup> each with dimensions of 8cm x 8cm x 70 cm located 5.8 meters from the interaction point. They are designed to measure the  $e^+e^- \rightarrow e^+e^-$  reaction at small angles. Scintillators in front of the lead glass define the acceptance and the lead glass counters measure the angle and energy of the electron pairs. In addition, the luminosity was also monitored with the L, A, B, C hodoscopes which measure the forward angle Bhabha scattering ( $\theta=12^\circ$  to  $26^\circ$ ). A very loose trigger was used which collects candidates for electron pairs, single-muon events, muon pairs, and hadron events. For electron pairs we require that opposite quadrants of A and B counters be in coincidence and that each quadrant has a minimum energy of 0.5 GeV. For single-muon events we require at least two A counters, two B counters, and one D counter to be triggered. For muon pairs we require at least two A counters in coincidence with a pair of opposite-quadrant D counters. For hadrons we require at least four A counters and three B counters, and each triggered quadrant A, B,

C to be in coincidence with the opposite quadrant.

Most of the cosmic ray and accidental events were rejected by requiring the event trigger to be within 15 nsec of the beam bunch signal. The trigger rate is typically 5 per second. A microprocessor is used to require that the S and T chambers have at least three counts for hadron triggers. This reduces the tape writing rate by a factor of 3.

The total energy of each interaction and the direction of a particle or group of particles was computed from the time and pulse height information of the shower counters and calorimeter counters. From the difference in time between the two phototubes of each shower counter and from the ratio of their pulse heights, we obtain two measurements of the position along the beam direction at which the particle struck the counter. The algorithms used were developed from analysis of test beam data which was accumulated for incident electrons and pions between 0.5 and 10 GeV. The azimuthal position was determined by the finely segmented shower counters. This method enables us to determine the  $\theta$  and  $\phi$  angles with an error of less than  $5^\circ$  for e or  $\gamma$  and less than  $15^\circ$  for hadrons.

#### Tests of Quantum Electrodynamics and of Universality for Charged Leptons

There have been many experiments testing quantum-electrodynamics with electrons and muons at electron-positron storage rings. The most notable experiments were done by Alles-Borelli et al.<sup>4)</sup>, Newman et al.<sup>5)</sup>, Augustin et al.<sup>6)</sup>, O'Neill et al.<sup>7)</sup>, and by our group at PETRA<sup>8)</sup> up to a center of mass energy of 17 GeV. For a good review of QED work see Brodsky and Drell<sup>9)</sup>. Much has been learned about the properties of the heavy lepton  $\tau$  since the original search began at ADONE on  $e^+ + e^- \rightarrow \mu e + \dots$ <sup>10),34)</sup>. The discovery of the  $\tau$  lepton at SLAC<sup>11)</sup> and its subsequent confirmation at DESY<sup>12)</sup> has inspired further studies. We know it is a spin 1/2 particle which decays weakly<sup>13)</sup> and whose properties are very similar to the muon.

In this experiment we study the reactions

$e^+ + e^- \rightarrow \ell^+ + \ell^-$  ( $\ell = e, \mu, \tau$ ) by simultaneously measuring their energy or angle dependence at various PETRA energies. These measurements enable us to compare the data with predictions of quantum electrodynamics, to test the universality of these leptons at very small distances, and to set a limit on the charged radius of these particles. Up to the present time, these reactions viz:

$$e^+ + e^- \rightarrow e^+ + e^- \text{ (Bhabha scattering)} \quad (1)$$

$$e^+ + e^- \rightarrow \mu^+ + \mu^- \quad (2)$$

$$e^+ + e^- \rightarrow \begin{array}{l} \tau^+ + \tau^- \\ \downarrow \\ \mu^+ + \nu's \end{array} \text{ (h or e) + } \nu's \quad (3)$$

have been measured simultaneously at the center of mass energies  $\sqrt{s} = 13, 17, 27.4,$  and 30 and 31.6 GeV.

#### Bhabha Scattering

The Bhabha events are identified by requiring two back-to-back showers which are collinear to within  $20^\circ$  in  $\phi$  and  $\theta$  and with a measured total shower energy greater than 8 GeV. For each particle, or particles, emitted within a cone of  $20^\circ$  which were not separable in the counters, the vector momentum was computed from pulse-height and counter-position information using the position of the interaction region (which is known to an accuracy of  $\pm 2$  cm by fitting tracks in the chambers for  $e^+e^- \rightarrow \mu^+\mu^-$  events). Photons emitted close to either electron are included in the fitted electron momentum. In Fig. 5 we show the measurement of the acoplanarity angle  $\Delta\theta$ . Because there are few events near the  $20^\circ$  cut and a very similar acoplanarity spectrum in  $\phi$ , we conclude that the background to elastic scattering events is negligible. The test beam data mentioned above yield a resolution on the energy sum of

$$\Delta E/E = 12\% / \sqrt{E} .$$

To eliminate most of the background from hadron jets, the energy in the K counters was required to be less than 7% of the total energy. Because the QED test is most sensitive to background in the large angle region, all events having  $\theta$  larger than  $60^\circ$  were scanned

on graphic displays which showed the distribution of counter hits. On the basis of a Monte Carlo study of hadron events, we conclude that the background from this source is less than 1% of these events.

The acceptance for  $e^+e^- \rightarrow e^+e^-$  was computed using a Monte Carlo technique and is defined by the geometry of the first shower counter A. Both energy and acceptance losses in the corners were found to be small.

The first-order QED photon propagator produces an  $s^{-1}$  dependence in the  $e^+e^- \rightarrow e^+e^-$  cross section. The quantity  $s \frac{d\sigma}{d\cos\theta}$  vs  $\cos\theta$  is independent of  $s$ . The distribution is plotted for the data at  $\sqrt{s} = 13, 17,$  and 27.4 GeV in Fig.6. Excellent agreement with QED predictions is seen. To express this agreement analytically, we compare our data with the QED cross section in the following form (since charge is not distinguished here):

$$\frac{d\sigma}{d\Omega} = \frac{\alpha^2}{2s} \left\{ \frac{q'^4 + s^2}{q^4} |F_S|^2 + \frac{2q'^4}{q^2 s} \text{Re}(F_S F_T^*) \right. \\ \left. + \frac{q'^4 + q^4}{q^2} |F_T|^2 + \frac{q'^4 + s^2}{q^4} |F'_S|^2 + \frac{2q^4}{q'^2 s} \text{Re}(F'_S F_T^*) \right. \\ \left. + \frac{q'^4 + q^4}{s^2} |F_T|^2 \right\} \{1+C(\theta)\},$$

where

$$F_S = 1 - \bar{q}^2 / (q^2 - \Lambda_{S\pm}^2)$$

is the form factor of the spacelike photon,

$$F'_S = 1 + \bar{q}'^2 / (q'^2 - \Lambda_{S\pm}^2),$$

$$F_T = 1 - \bar{s} / (s - \Lambda_{T\pm}^2)$$

is the form factor of the timelike photon  $q^2 = s \cos^2(\theta/2)$ ,  $q'^2 = s \sin^2(\theta/2)$ ,  $\Lambda$  is the cut-off parameter in the modified photon-propagator model<sup>14)</sup> and  $C(\theta)$  is the radiative correction term as a function of  $\theta$ .

The radiative correction on the  $e^+e^-$  elastic process was calculated using a modified program from Berends<sup>15)</sup> which includes the contribution of the heavy-lepton ( $\tau$ ) loop and the hadronic vacuum polarization. The inclusion of these two effects changes the radiative correction from minus a few percent, as was commonly used previously, to, for example, + 4.6% at  $\theta = 14^\circ$  and + 1.3% at  $\theta = 90^\circ$  for  $\sqrt{s} = 17$  GeV. It is slightly

smaller at  $\sqrt{s} = 13$  GeV.

In order to estimate the  $\Lambda$  parameters a Monte Carlo program was used to generate  $e^+e^-$  pairs which were then traced through the detector with the inclusion of measured  $\theta$ ,  $\phi$  resolutions. A  $\chi^2$  fit to all of the 13, 17 and 27 GeV data was then made using this Monte Carlo-generated angular distribution. The normalization was treated in two ways: (1) the total number of Monte Carlo events in the region  $0.9 < \cos\theta < 0.98$  was set equal to the total number of measured events in the same region, (2) the minimum- $\chi^2$  for the entire data sample determined the normalization. The two methods agree with each other to within 3% and give essentially the same result in the cut-off parameter  $\Lambda$ . The lower limits of  $\Lambda$  at 95% confidence level under various assumptions are shown in the following table:

Cut-off GeV

$\Lambda$	$1 - \frac{q^2}{q^2 - \Lambda^2}$	$1 + \frac{q^2}{q^2 - \Lambda^2}$
$\Lambda_S$	52	55
$\Lambda_T$	60	52
$\Lambda_S = \Lambda_T$	65	64

#### Universality<sup>16)</sup>

The  $\mu^+\mu^-$  from reaction (2) is easily identified by coplanarity, collinearity and momentum conservation. The acceptance for  $\mu^+\mu^-$  production is 0.41, with a systematic error of 0.03, at all energies.

We obtained the cross section  $e^+e^- \rightarrow \tau^+\tau^-$  by detecting  $\mu$  + hadron (or  $\mu$  + electron) final states from (3) and using the known branching ratio of  $\tau \rightarrow \mu + \nu + \bar{\nu}$  (16%) and  $\tau \rightarrow (e, lh, \text{ or multihadrons}) + \nu$ 's (84%)<sup>13)</sup>. The muon in reactions (3) and (2) is required to penetrate  $> 1$  m magnetized iron to reach the outside muon chamber P. This presents the following kinematic restriction on the muon:  $45^\circ < \theta_\mu < 135^\circ$  and  $P_\perp > 1.5$  GeV. For reaction (3) the total energy of the hadrons (or electrons) is required to be greater than 2 GeV.

The major background to reaction (3) is

the two-photon process

$$e^+ + e^- \rightarrow e^+ + e^- + \mu^+ + \mu^- \quad (4).$$

This process becomes important at high energies because the total cross section over  $4\pi$  steradians grows as  $\ln(\sqrt{s}/m_e)^2 \ln(\sqrt{s}/m_\mu)$  with increasing beam energy in contrast to reaction (3) whose rate is expected to fall as  $1/s$ . The observed cross section for the two-photon process is suppressed by a factor  $\sim 10^3$  relative to the total cross section by momentum cuts on the muons and by energy and angle cuts on the electrons, but the accepted event rates remain significant. In Fig. 7 we show the calculated cross section in our detector when the observed particles are

- (a) two  $\mu$ 's only,
- (b) only one  $\mu$  and one  $e$  and,
- (c) two  $\mu$ 's and one  $e$ .

The cross sections for each of these configurations were computed using a Monte Carlo integration program by Vermaseren<sup>17)</sup>, which incorporates the exact QED matrix elements to order  $\alpha^2$ . The computations were checked by comparing them to the cross sections measured for reaction (4) using the following cuts:

$$\begin{aligned} 168^\circ &\geq \theta_e \geq 12^\circ & E_e &\geq 2 \text{ GeV} \\ 135^\circ &\geq \theta_{\mu_1} \geq 45^\circ & P_{\perp\mu_1} &\geq 1.5 \text{ GeV (first muon)} \\ 147^\circ &\geq \theta_{\mu_2} \geq 33^\circ & P_{\perp\mu_2} &\geq 0.8 \text{ GeV (second muon)}. \end{aligned}$$

The measured cross sections, also shown in Fig. 7, agree well with the calculations in all cases.

The cross section for case (a) is much larger than that for the process

$$e^+ + e^- \rightarrow \tau + \bar{\tau} \rightarrow \mu^+ + \mu^- + 4\nu,$$

and the  $2\mu$  events from the two processes are hard to distinguish. We therefore exclude case (a) from the sample of  $\tau\bar{\tau}$  candidates. In case (b) the electron from the two-photon process is strongly peaked in the small angle region. Typically,  $\frac{d\sigma_{\mu e}}{d(\cos\theta_e)}$  decreases by two orders of magnitude from  $\cos\theta_e = 0.98$  to 0.80. Furthermore, the observed muons and electrons tend to be coplanar because of conservation of transverse momentum. By

requiring  $30^\circ < \theta_e < 150^\circ$  for the  $\tau\bar{\tau}$  sample, we are able to reduce the two-photon contribution to a negligible level ( $< 10^{-3}$  picobarns). The rate for case (c) is small and can be readily separated from the  $\tau$  events.

We remark that the  $\mu$ -hadron events produced by reaction (1) in our energy region are almost collinear. This kinematic fact can be used to readily distinguish reaction (1) from  $\mu$ -hadron events produced by the semi-leptonic decay of particles with c(charm) or b(beauty) quantum number. In the latter cases the muon and its accompanied hadrons are emitted closely together.

The measured muon momentum and hadron energy for the  $\tau\bar{\tau}$  candidates is in agreement with calculations based on the known decay properties of the  $\tau$  lepton<sup>13)</sup>.

The acceptance is calculated using a Monte Carlo method to generate  $\tau\bar{\tau}$  production from reaction (3) including radiative corrections. We obtain a detection efficiency of  $\sim 10\%$  for  $\tau$  pairs at various energies.

The resultant  $e^+e^- \rightarrow \mu^+\mu^-$  and  $\tau\bar{\tau}$  cross section as a function of  $\sqrt{s}$  is plotted in Figs. 8a + 8b together with the QED prediction. We see that from  $q^2=s=169$  to  $q^2=999$  GeV<sup>2</sup> the data agree well with the predictions of QED for the production of a pair of point like particles. To parameterize the size (radius) of the particles we take a form factor of the following functional dependence:

$$F_\ell = 1 + \frac{q^2}{q^2 - \Lambda_{\ell\pm}^2} \quad (\ell = e, \mu, \tau)$$

Comparing our data with this form factor yields the following table of cut-off parameters (at 95% confidence level in GeV):

Cut-off GeV

$\ell$	electron	muon	tau
$\Lambda_-$	95	97	53
$\Lambda_+$	74	71	47

Thus, to a radius  $< \sim 10^{-16}$  cm, all the known charged leptons are pointlike particles in their electromagnetic interactions.

## Hadron Final States<sup>18)</sup>

To eliminate the bulk of the beam-gas background, which is mainly low energy and one sided, we first require that the total energy deposited in the calorimeter be greater than half of the total center of mass energy, and that the computed total  $P_{//}$  and total  $P_{\perp}$  each be less than 50% of the observed energy. One part in a thousand of the raw events pass the above criteria, and pictures of each surviving event were scanned by physicists on a video screen to assure that the counter tracks are reasonably fitted. We further demand at least one track in the drift chambers pointing back to the interaction region to distinguish hadronic events from beam-gas events. To discriminate against events of electromagnetic origin such as  $ee \rightarrow ee$ ,  $ee \rightarrow ee \gamma$ , and so forth, we have accepted three types of events with different shower properties which are as follows:

(1) two narrow showers penetrating into the third and fourth layers of the hadron calorimeter counters (K). There is a total of 33 radiation lengths from the interaction region. To discriminate against  $e^+e^-$  and  $\gamma\gamma$  final states, the total energy in the K calorimeter counters is required to be greater than 7% of the total shower energy in A + B + C.

(2) Two broad showers penetrating into the first or second layer of the K calorimeter counters with energy greater than 1% of the total A, B and C shower energy.

(3) Three or more broad showers with tracks in the drift chambers are also considered.

The energy spectrum of the events passing the cut is shown as the non-hatched area of Fig. 9. The energy spectrum of beam-gas events, which are defined by having a chamber track missing the interaction point by at least 15 cm from the intersection point, is shown as the hatched area in Fig. 9. A comparison of these two spectra (which were taken simultaneously) shows that the real hadron events can be readily separated from beam-gas events by an energy cut. Such an energy cut also reduces the contamination from two-photon processes and  $e^+e^- \rightarrow \tau^+\tau^-$

events which yield hadrons in the final state.

A Monte Carlo program was used to compute the acceptance for

$$e^+e^- \rightarrow \text{hadrons} \quad (5)$$

and to determine the contribution to our hadron event sample from the two-photon process

$$e^+e^- \rightarrow e^+e^- + \text{hadrons} \quad (6)$$

and

$$e^+e^- \rightarrow \tau^+\tau^- \quad (7)$$

The Monte Carlo program generates two jets for reaction (5) according to the Feynman-Field ansatz<sup>19)</sup> which include not only u, d and s quarks but also the contribution of c(charm) and b(bottom) quarks. The branching ratios for the decays of the D and F mesons rely either on available experimental data or otherwise on isospin-statistical models<sup>20)</sup>. The branching ratios for the decay modes of B mesons (from  $b\bar{b}$ ) and T mesons, which are yet to be observed, are based largely on the work of Ali et al.<sup>21)22)</sup> in the framework of the Kobayashi-Maskawa six-quark model<sup>23)</sup>. The probability of producing each quark flavor is taken to be proportional to the square of the quark charge q, with  $q_c=2/3$  and  $q_b=-1/3$ .

Acceptances for reaction (5) were computed using u, d, s, c, and b quarks only, with the mass of the B mesons taken to be in the range of 5-6 GeV, expected if the T is a  $b\bar{b}$  bound state. The production of top quark pairs was only considered in connection with the jet analysis of the events (described later), where the mass of the T meson was taken to be in the range of 9 to 13 GeV. Above this threshold the  $t\bar{t}$  production probability was assumed to be 4/15 of the total cross section. To improve the accuracy of the model computations for reaction (5), we incorporated initial radiative effects<sup>24),25)</sup>, in the computer program.

The generation of events for reaction (6) was performed in the equivalent-photon approximation with multipions only in the final states<sup>26)</sup>. Simulated events for reaction (7) were produced according to the "standard model", where the  $\tau$  is considered

as a sequential heavy lepton<sup>27)</sup>, as indicated by the available data<sup>28)</sup>.

The total cross section for  $e^+e^- \rightarrow \text{hadrons}$ , as expressed in terms of

$$R = \sigma(e^+e^- \rightarrow \text{hadrons}) / \sigma(e^+e^- \rightarrow \mu^+\mu^-),$$

is shown in Table I. Systematic errors due to model uncertainties for the acceptance of reaction (5) are 10% and the uncertainties in evaluating reactions (6) and (7) are limited by the lack of experimental data on high energy, high multiplicity states. The "27 GeV" data are the combination of data taken at two slightly different energies: 27.4 GeV and 27.7 GeV.

Fig. 10 summarizes the R value as measured by MARK-J at six different energies. No clear step of 1.3 units in R is observed up to 31.6 GeV as would be expected if the  $t\bar{t}$  threshold had been reached.

#### Jet Analysis<sup>18),29)</sup>

A jet analysis of the hadronic events was performed using the spatial distribution of the energy deposited in the detector. For each counter hit, a vector  $p^i$  is constructed, whose direction is given by the position of the signal in the counter, and magnitude by the corresponding deposited energy. The thrust parameter T is defined as:

$$T = \max. \left[ \frac{\sum |p_{//}^i|}{\sum |p^i|} \right]$$

where  $p_{//}^i$  is the parallel component of  $p^i$  along a given axis, and the maximum is found by varying the direction of this axis. The sums are taken over all counter hits.

The normalized thrust distributions  $\frac{1}{N} \frac{dN}{dT}$  for 13, 17, 22, the combination of 27.4 and 27.7 (labeled 27 GeV combined), 30, and 31.6 GeV data are shown in Figs. 11a + 11b along with the Monte Carlo predictions. (The individual distributions at 27.4 and 27.7 GeV are in agreement with each other).

As expected for production of final states with two jets of particles, the distributions peak at high T. The data are consistent with Monte Carlo distributions which include u, d, s, c, and b quarks. The 31.6 GeV data are also compared with a Monte Carlo calculation which includes a charge

2/3 t quark produced as described previously. The data are inconsistent with the production of such a new quark.

Fig. 12 shows the average thrust  $\langle T \rangle$  plotted at the six energies. The solid curves are from Monte Carlo calculations which include u, d, s, c, and b quarks with gluon emission. The energy dependences of the data are smooth, and show none of the steps which would have appeared at new quark thresholds.

Thus, within the limits of the model described earlier, our measurements of R and T all indicate that the production of a new charge 2/3 quark is unlikely up to 31.6 GeV C.M. energy. The production of a charge 1/3 quark can not be ruled out by the present data.

Fig. 11c shows the normalized thrust distributions at 27 combined, 30 and 31.6 GeV where the measured energy of the selected events is at least 70% of  $\sqrt{s}$ . The curves show the Monte Carlo predictions with and without inclusion of gluons. As can be seen, this data lends support to the necessity of including gluons in the Monte Carlo.

#### Discovery of Three Jet Events

An analysis of the distribution of hadronic energy in three dimensions was carried out in order to see the effects attributable to QCD, in particular, the emission of gluons<sup>29)</sup>. To describe the energy distribution, three orthogonal axes are defined for each event as follows:

(1) As before, the thrust axis is defined in the direction,  $\hat{e}_1$ , along which the projected energy flow is maximized. That is,

$$\text{Thrust} = \max. \frac{\sum_i |\vec{p}^i \cdot \vec{e}_1|}{\sum_i |\vec{p}^i|}$$

$\vec{p}^i$  is the energy flow detected by a counter as described before and  $\sum_i |\vec{p}^i|$  is the total visible energy,  $E_{\text{vis}}$ .

(2) To investigate the energy distribution in the plane perpendicular to the thrust axis, a second direction  $\vec{e}_2$  is defined perpendicular to  $\vec{e}_1$ , it is the direction along which the projected energy

flow momentum in that plane is maximized. The quantity "Major" is defined as:

$$\text{Major} = \max. \frac{\sum_i |\vec{p}^i \cdot \vec{e}_2|}{E_{\text{vis}}}; \quad e_2 \perp e_1.$$

(3) The third axis,  $\vec{e}_3$ , is orthogonal to both the thrust and the major axes. It is found that the absolute sum of the projected energy flow along this direction called "Minor", is very close to the minimum of the momentum projection along any axis, i.e.

$$\text{Minor} \sim \min. \sum_i \frac{|\vec{p}^i \cdot \vec{e}_3|}{E_{\text{vis}}}$$

If hadrons were produced according to phase space or  $q\bar{q}$  two-jet distribution, the energy distribution in the plane defined by the major and minor axes would be isotropic, and the difference between the major and the minor (hereafter referred to as "oblateness") should be small. On the other hand, if hadrons are produced via three-body intermediate states such as  $q\bar{q}g$ , and if each of the three bodies fragments into a jet of particles with  $\langle P_{\perp} \rangle \sim 325$  MeV, then by conservation of momentum, the energy distribution of these events would be oblate. The quantity oblateness is defined as

$$\text{Major} - \text{Minor}.$$

The oblateness is  $\sim \frac{2\langle P_{\perp} \rangle_{\text{gluon}}}{\sqrt{s}}$  for three-jet final states and is  $\sim 0$  for final states coming from two jets or phase space distribution. According to QCD<sup>29)</sup>, oblateness should increase at higher energies and at lower thrust values. The quantity oblateness is particularly suited to display the effect of gluon emission because it is rather insensitive to the detailed assumptions of QCD-based models, such as the precise  $p_{\perp}$  distribution of the hadrons and the fragmentation functions<sup>29)</sup>.

Fig. 13 shows the measured energy dependence of the oblateness as compared to the prediction of the  $q\bar{q}g$  model<sup>29)</sup> as well as the  $q\bar{q}$  model. We see that at low energies, the data are in agreement with both models, while at higher energies  $27.4 \leq \sqrt{s} \leq 32$  GeV, the data agree better with the  $q\bar{q}g$  calculation, and are quite inconsistent with

the naive  $q\bar{q}$  predictions. This is expected in QCD since more and more hard gluons are emitted as energy increases.

To check the dependence of oblateness on the  $P_{\perp}$  distribution of the hadrons and the behaviour of the fragmentation function  $D(Z)$ , (where  $Z = \frac{P_h}{P_q}$ ), we have calculated, at  $\sqrt{s} = 30$  GeV, the change in the average oblateness,  $\langle O \rangle$ , by changing the  $\langle P_{\perp} \rangle$  from the commonly used value of 325 MeV to  $\langle P_{\perp} \rangle = 425$  MeV, or by changing  $D(Z) = (1-Z)^2$  to  $D(Z) = \text{constant}$  for the C(charm)<sup>30)</sup> and B(bottom) quarks. In both cases the  $\langle O \rangle$  changes by  $0.002 \pm 0.002$ .

Fig. 14 shows the measured oblateness versus thrust for the combined data at  $\sqrt{s} = 27.4, 30,$  and  $31.6$  GeV. We see that for lower values of thrust the oblateness of the energy distribution increases.

Fig. 15a shows the event distribution as a function of oblateness for the data at  $\sqrt{s} = 17$  GeV where the gluon emission effect is expected to be small. The data indeed agree with both models, although the prediction with the gluon is still preferred.

Fig. 15b shows the event distribution as a function of oblateness for the data at  $27.4 \leq \sqrt{s} \leq 31.6$  GeV as compared with the predictions of  $q\bar{q}g$  models. Again, in the  $q\bar{q}$  model we use both  $\langle P_{\perp} \rangle = 325$  MeV and  $\langle P_{\perp} \rangle = 425$  MeV. The data have more oblate events than the  $q\bar{q}$  model predicts, but agree with the  $q\bar{q}g$  model very well.

To see the detailed structure of the jets we further divide the energy distribution of each event into two hemispheres using a plane defining the Major and Minor axes. The forward hemisphere contains the narrow jet and the other contains the broader jet. The major, the minor and the oblateness are calculated separately for each hemisphere. A sample of the events with low thrust and high oblateness, where the gluon emission effect is expected to be relatively large, is selected for detailed examination. The sum of the angular energy distribution of all events at  $\sqrt{s} = 27.4, 30,$  and  $31.6$  GeV with the thrust  $< 0.8$  and the oblateness of the broad jet  $> 0.1$  is shown in Fig. 16. We see in Fig. 16a that the accumulated energy

distribution in the plane defined by the thrust and the major shows three distinct jets which up to now have not been observed<sup>31)</sup>. The longest jet is pointing along the thrust axis and the opposite hemisphere actually contains two smaller jets with a large angle between them. We have oriented the two small jets according to their sizes<sup>33)</sup>. The calculated energy distribution using the  $q\bar{q}g$  model is shown in Fig. 16 and is compatible with the data; the  $\chi^2$  is 67 for 70 degrees of freedom. In Fig. 16b we show the accumulated energy distribution in the thrust-minor plane. The flat distribution is again consistent with the  $q\bar{q}g$  predictions.

In summary we have shown that the energy flow of hadronic events from  $e^+e^-$  interactions can be described in terms of QCD. The effects are particularly striking when the data is expressed in terms of the quantity "oblateness". The average oblateness as a function of thrust and  $\sqrt{s}$ , and the differential oblateness distributions all favor the descriptions including gluon emission. The effect clearly increases with increasing energy. Furthermore, the energy distribution of the events with thrust  $< 0.8$  and oblateness  $> 0.1$  shows three distinct jet structures which is in agreement with the prediction of the  $q\bar{q}g$  models.

#### Acknowledgements

We wish to thank Professor H. Schopper and Professor G. Voss who made the experiment possible. We are grateful for the cooperation of the Minister für Forschung und Technologie of the Federal Republic of Germany, the Joint Research Program of FOM and ZWO of The Netherlands, the United States Department of Energy, and the Institute of High Energy Physics of the Chinese Academy of Science in this endeavor. We especially thank Professors A.N. Diddens, H. Feshbach, E. Lohrmann, F. Low, Drs. F.J. Eppling and G. Söhngen for their valuable advice and support and Professors S. Glashow, H. Georgi, T.D. Lee, Drs. A. Ali and T. Walsh for helpful discussions. In

addition we thank Miss. I. Schulz, Miss. S. Marks, Mrs. S. Burger, Miss P. Reddick, Messrs. P. Berges, J.F. Donahue and D. Osborne for technical and administrative help. We thank Drs. H. Dilcher, D. Hubert, G. Kessler, J. Kouptsidis, F. Schwickert, Messrs. N. Feind, W. Hoppe, K. Löffler, R. Siebels and E. Weiss for their valuable assistance. We also thank our technicians from the III. Physikalisches Institut A, Aachen, including Messrs. K. Bosseler, K. Dahmen, J. Dickmeis, H. Frohn, J. Grooten, H.D. Hilgers, G. Hilgers, R. Pahlke, W. Reuter and C. Schölgens, and thank the staff of the Laboratory for Nuclear Science at MIT, including Mrs. Distefano, Mrs. J. Flanagan, Mrs. J. Hudson, Mrs. G. Mitchell, Messrs. R. Adams, R. Calileo, T. DeChicco and C. Tourtelotte for their dedicated services which contributed to the efficient installation and smooth operation of the experiment.

#### References

- 1) U. Becker et al., Nucl. Instrum. Methods 128, 593 (1975).
- 2) D. Antreasyan et al., in Proceedings of the 19th International Conference on High Energy Physics, Tokyo, Japan, August 1978 (to be published).
- 3) P.D. Luckey et al., in Proceedings of the International Symposium on Electron and Photon Interactions at High Energies, Hamburg, 1965 (Springer, Berlin, 1965), Vol. II, p. 423.
- 4) V. Alles-Borelli et al., Nuovo Cimento 7A, 345 (1972).
- 5) H. Newman et al., Phys. Rev. Lett. 32, 483 (1974).
- 6) J.E. Augustin et al., Phys. Rev. Lett. 34 233 (1975).
- 7) L.H. O. Neill et al., Phys. Rev. Lett. 37 395 (1976).
- 8) D.P. Barber et al., Phys. Rev. Lett. 42, 1113 (1979).
- 9) D. P. Barber et al., to be published.
- 10) S.J. Brodsky and S.D. Drell, Annu. Rev. Nucl. Sci. 20, 147 (1970).
- 11) ADONE Proposal INFN/AE-67/3, March 1967, ADONE-Frascati (unpublished) and M. Bernardini et al., (Zichichi group) Nuovo Cimento 17A, 383 (1973).
- 12) M. Perl et al., Phys. Rev. Lett. 35, 1489 (1975).
- 13) G. Feldman et al., Phys. Rev. Lett. 38, 117 (1977).
- 14) J. Burmester et al., Phys. Lett. 68B, 297 (1977).
- 15) J. Burmester et al., Phys. Lett. 68B, 301 (1977).
- 16) For a review of our present knowledge of the  $\tau$  lepton see Günter Flügge, Z. Physik C, Particles and Fields 1, 121-138 (1979).
- 17) S.D. Drell, Ann. Phys. (N.Y.) 4, 75 (1958).
- 18) T.D. Lee and G.C. Wick, Phys. Rev. D 2, 1033 (1970).
- 19) F.A. Berends et al., Phys. Lett. 63B, 432 (1976) and private communication. We wish to thank Dr. Berends for providing us with his up-to-date computer program for our experiment.
- 20) D.P. Barber et al., M.I.T. Laboratory for Nuclear Science Report 105, August 1979.
- 21) J.A.M. Vermaseren, CERN, to be published. We wish to thank Dr. Vermaseren for helpful assistance.
- 22) D.P. Barber et al., M.I.T. Laboratory for Nuclear Science Reports 103 - 104 (1979).
- 23) R.D. Field and R.P. Feynman, Nuclear Physics B136, 1 (1978).
- 24) M.K. Gaillard, B.W. Lee, and J.L. Rosner, Rev. Mod. Phys. 47, 277 (1975).
- 25) C. Quigg and J.L. Rosner, Phys. Rev. D17, 239 (1978).
- 26) A. Ali, J.G. Koerner, G. Kramer, and J. Wilrodt, DESY Reports 78/51 and 78/67 (1978), unpublished.
- 27) A. Ali, Z. Physik C, Particles and Fields, 1, 25 (1979).
- 28) A. Ali and E. Pietarinen, DESY-Report 79/12 (1979), unpublished.
- 29) M. Kobayashi and T. Maskawa, Prog. Theor. Phys. 49, 652 (1973).
- 30) G. Bonneau and F. Martin, Nuclear Physics B27, 381 (1971).

- 25) Y.S. Tsai, Rev. Mod. Phys. 46, 815 (1974).  
L.W. Mo and Y.S. Tsai, Rev. Mod. Phys. 41, 205 (1969).
- 26) H. Terazawa, Rev. Mod. Phys. 45, 615 (1973).  
We used  $\sigma(\gamma\gamma \rightarrow \text{multipion}) = |240 - 270/W^2| \text{nb}$ .  
W is the energy of the two-photon system.
- 27) Y.S. Tsai, Phys. Rev. D4, 2821 (1971).  
H.B. Thacker and J.J. Sakurai, Phys. Lett. 36B, 103 (1971).  
K. Fujikawa and N. Kawamoto, Phys. Rev. D14, 59 (1976).
- 28) M.L. Perl, in Proceedings of the 1977 Symposium on Lepton and Photon Interactions at High Energies, Hamburg, edited by F. Gutbrod (Deutsches Elektronen-Synchrotron, Hamburg, 1977), p. 145.
- 29) J. Ellis et al., Nucl. Phys. B111, 253 (1976).  
T. DeGrand et al., Phys. Rev. D16, 3251, (1977).  
A. DeRujula et al., Nucl. Phys. B138, 387 (1978).  
B.A. Gordon, Phys. Rev. Lett. 41, 615 (1978).  
G. Kramer et al., Phys. Lett. 79B, 249 (1978).  
S.I. Eidelman et al., Phys. Lett. 82B, 278 (1979).  
PLUTO Collaboration, Phys. Lett. 82B, 449 (1979).  
J.G.H. DeGroot et al., Phys. Lett. 82B, 456 (1979).  
J.G.H. DeGroot et al., Phys. Lett. 82B, 292 (1979).  
C. Bromberg et al., Phys. Rev. Lett. 43, 565 (1979).  
P. Hoyer et al., DESY-Preprint 79/21, April 1979.  
S. Brandt, paper presented at the EPS International Conference on High Energy Physics, Geneva, 27 June-4 July 1979. Also DESY-Preprint 79/43, July 1979.
- P. Söding, invited talk at the EPS International Conference on High Energy Physics, Geneva, 27 June - 4 July 1979.
- R. Cashmore, paper presented at the EPS International Conference on High Energy Physics, Geneva, 27 June - 4 July 1979.
- H. Georgi, Private Communication.  
D.P. Barber et al., Phys. Lett. 85B, 463 (1979).  
D.P. Barber et al., M.I.T. Laboratory for Nuclear Science Report 106, August 1979. To be published in Physical Review Letters.
- See also papers by JADE, PLUTO, and TASSO groups at the 1979 International Symposium on Lepton and Photon Interactions at High Energies, August 23-29, 1979, Batavia, Illinois, U.S.A.
- See also Report by TASSO, DESY-Report 79-53 (1979).
- 30) We have adopted the notation that Z equals a fraction of quark energy carried away by the hadron.
- 31) Phase space distribution will show three nearly identical lobes due to the method of selection used. However, at  $\sqrt{s} = 30$  GeV these lobes are very different in appearance from the jet shown in Fig. 16. In general, one expects the three jets from  $q\bar{q}g$  to become slimmer and easier to distinguish from the phase space distribution as the center of mass energy increases. Using a  $\chi^2$  fit of the phase space energy distribution to the data we found that  $\chi^2 = 222$  for 77 degrees of freedom. Therefore, the phase space is inconsistent with the data. Furthermore, large contributions of phase space distributions are ruled out by our data on thrust distribution (see references 32, 18).

- 32) D.P. Barber et al., Phys. Rev. Lett. 42, 1110 (1979).
- 33) In general the smallest jet came from gluon fragmentation.
- 34) S. Orito et al., Phys. Lett. 48B, 164 (1974).

#### Table Captions

Table I Values of  $R = \sigma(e^+e^- \rightarrow \text{hadrons}) / \sigma(e^+e^- \rightarrow \mu^+\mu^-)$

#### Figure Captions

- Fig. 1 End view of the MARK-J detector.
- Fig. 2 Side view of the MARK-J detector.
- Fig. 3 A photograph of the detector taken shortly after its installation in the final position.
- Fig. 4 A photograph of the detector after a rotation around the beam axis.
- Fig. 5 The measured acoplanarity angle  $\Delta\theta$  for Bhabha events at  $\sqrt{s} = 17$  GeV.
- Fig. 6 The  $e^+e^- \rightarrow e^+e^-$  data for  $\sqrt{s} = 13$  GeV, 17 GeV, and 27.4 GeV compared with the prediction from QED.
- Fig. 7 The observed cross section of  $e^+e^- \rightarrow e^+e^-\mu^+\mu^-$  in our detector as a function of  $\sqrt{s}$  when the observed particles are:
- (a) two  $\mu$ 's
  - (b) one  $\mu$  and one e
  - (c) two  $\mu$ 's and one e.
- The solid lines are Monte Carlo calculations of the yield from two-photon diagrams and the points are our measurements.
- Fig.8a The measured and predicted total cross section of  $e^+ + e^- \rightarrow \mu^+ + \mu^-$ .
- Fig.8b The measured  $e^+ + e^- \rightarrow \tau^+ + \tau^-$  cross section as a function of  $\sqrt{s}$ . The curve is the same as in Fig, 8a.
- Fig. 9 Nonhatched area: energy spectra of the hadron events passing the criteria as defined in the text. Hatched area: energy spectrum of the beam-gas events.
- Fig.10 R values measured by MARK-J. The errors are statistical only. There is

an additional 15% systematic error on each measured point.

Fig.11a The thrust distribution  $\frac{1}{N} \frac{dN}{dT}$  at a)  $\sqrt{s} = 13$  GeV, b)  $\sqrt{s} = 17$  GeV, and c)  $\sqrt{s} = 22$  GeV. The curve is the Monte Carlo prediction based on u, d, s, c, and b quarks. In this plot the visible energy is at least 50% of  $\sqrt{s}$ .

Fig.11b The thrust distribution  $\frac{1}{N} \frac{dN}{dT}$  at  $\sqrt{s} = 27$  GeV combined,  $\sqrt{s} = 30$  GeV, and  $\sqrt{s} = 31.6$  GeV. The solid curve is the Monte Carlo prediction based on u, d, s, c, and b quarks. The dotted curve in the 31.6 data has the t quark contribution. In this plot the visible energy is at least 50% of  $\sqrt{s}$ .

Fig.11c The thrust distribution  $\frac{1}{N} \frac{dN}{dT}$  at  $\sqrt{s} = 27, 30, 31.6$  GeV showing the comparison of the data with the Monte Carlo with and without gluons. In this plot the visible energy is at least 70% of  $\sqrt{s}$ .

Fig.12 The average thrust as a function of  $\sqrt{s}$ , the C.M. energy. The curve is the Monte Carlo prediction based on u, d, s, c, and b quarks with gluon emission.

Fig.13 The average oblateness,  $\langle O \rangle$ , as a function of  $\sqrt{s}$  compared with the predictions of  $q\bar{q}$  (dashed curve) and  $q\bar{q}g$  model (solid curve). Also shown at  $\sqrt{s} = 30$  GeV in the  $q\bar{q}$  model calculation under two different conditions:

Point X:  $\langle P_{\perp} \rangle = 325$  MeV  
 $D(Z) = (1-Z)^2$

Point Y:  $\langle P_{\perp} \rangle = 425$  MeV  
 $D(Z) = \text{Constant for B and C quarks.}$

Fig.14 The average oblateness at 27.4-31.6 GeV as a function of thrust compared with the predictions of  $q\bar{q}$  and  $q\bar{q}g$  model.

Fig.15a The distribution  $\frac{1}{N} \frac{dN}{dO}$  as a function of oblateness at  $\sqrt{s} = 17$  GeV.

Fig.15b The distribution  $\frac{1}{N} \frac{dN}{dO}$  as a function of oblateness at  $\sqrt{s} = 27.4-31.6$  GeV.

In both figures 15a and 15b the solid curves are the predictions based on the  $q\bar{q}g$  model and the dashed curve based on the standard  $q\bar{q}$  model with  $\langle P_{\perp} \rangle = 325$  MeV. The dash dotted curve in Fig. 15b is the  $q\bar{q}$  model prediction with  $\langle P_{\perp} \rangle = 425$  MeV.

Fig.16a A polar plot of the energy distribution in the plane defined by the thrust and the major axes for all the events with thrust  $< 0.8$  and oblateness  $> 0.1$  at  $\sqrt{s} = 27.4, 30,$  and  $31.6$  GeV. The energy value is proportional to the radial distance. The superimposed dashed line is the distribution calculated using  $q\bar{q}g$  model.

Fig.16b The measured and calculated energy distribution in the plane defined by the thrust and the minor axes.

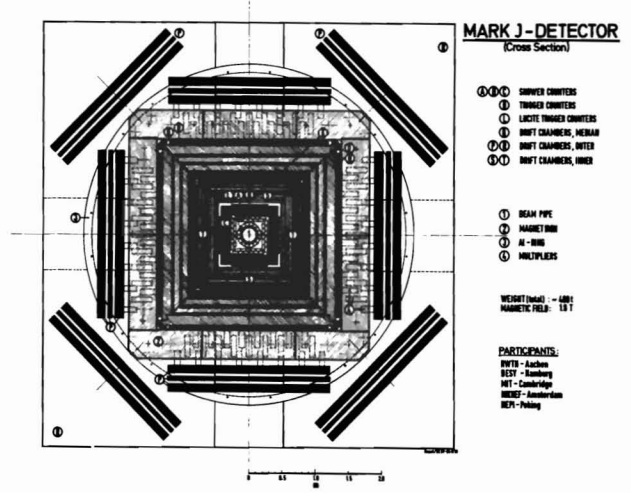


Fig. 1

$E_{CM}$	MARK J $\int Ldt$ ( $nb^{-1}$ )	R-values		
		EVENTS	R $\pm$ STAT. ERROR	SYSTEM. ERROR
13	53	98	$4.6 \pm 0.5$	0.7
17	60	68	$4.9 \pm 0.6$	0.7
22	50	42	$4.7 \pm 0.7$	0.7
27 combined	508	216	$3.8 \pm 0.3$	0.6
30	604	254	$4.2 \pm 0.3$	0.6
31.6	243	88	$4.0 \pm 0.5$	0.6

**CORRECTIONS**

- ACCEPTANCE : 80% typical
- $e^+e^- \rightarrow \tau^+ \tau^-$  :  $\Delta R \approx -0.3$
- $e^+e^- \rightarrow e^+ e^- + \text{hadrons}(2Y)$   $\Delta R \approx -0.1$
- Radiative Corrections -8 to -10%

TABLE 1

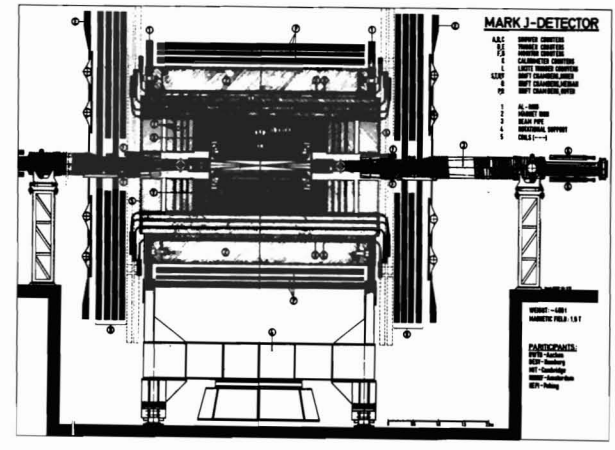


Fig. 2

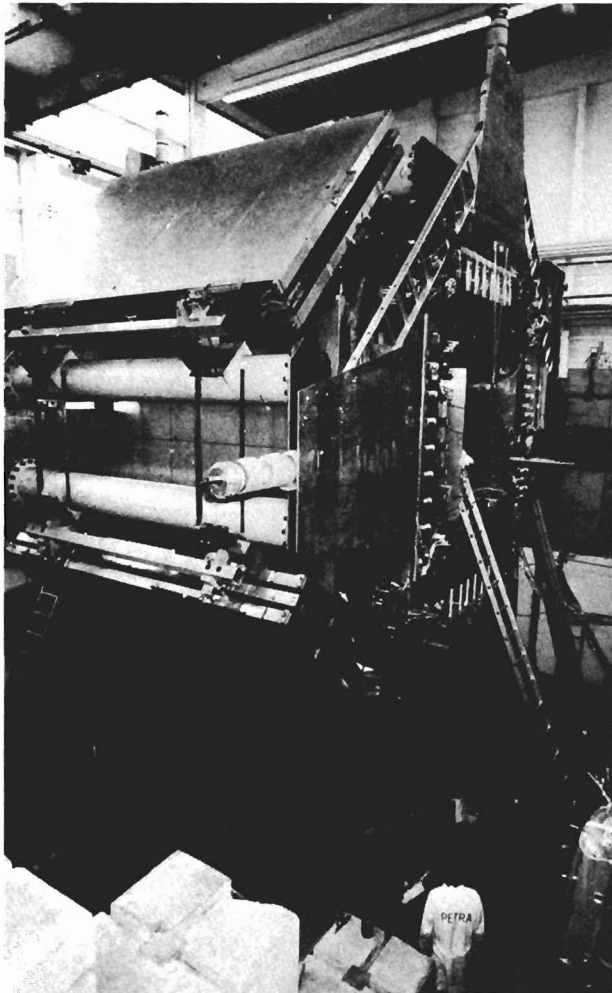


Fig. 3

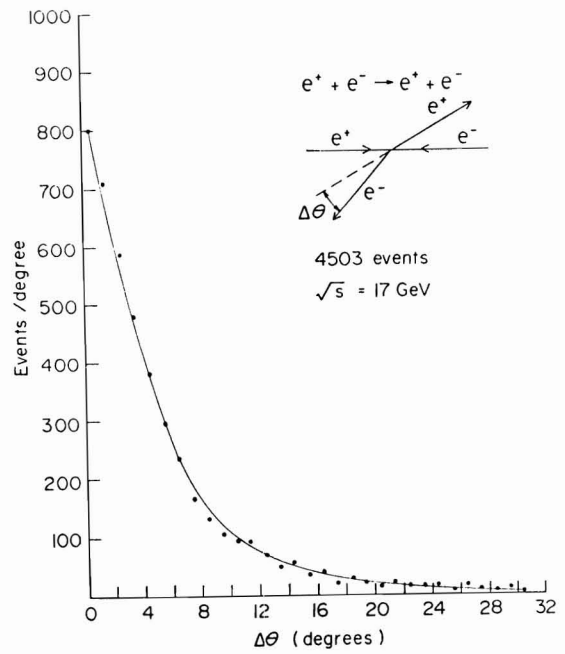


Fig. 5

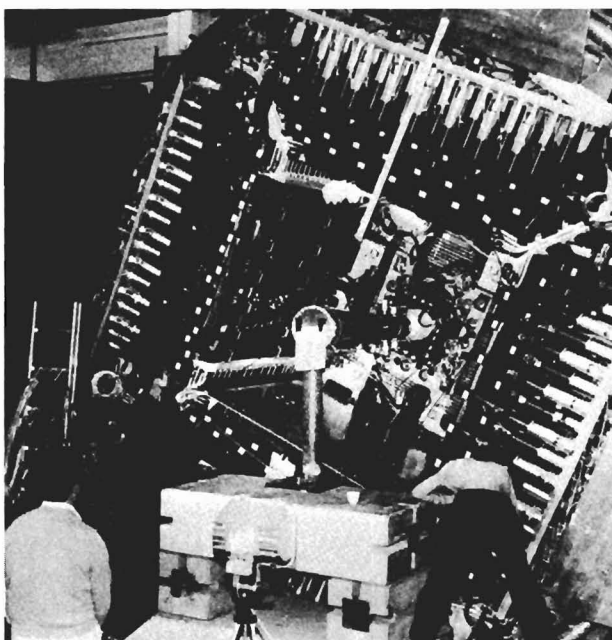


Fig. 4

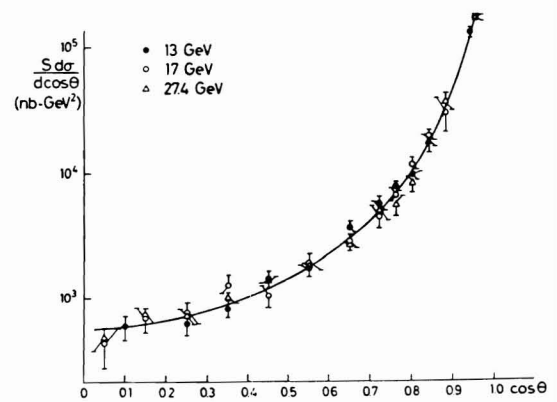


Fig. 6

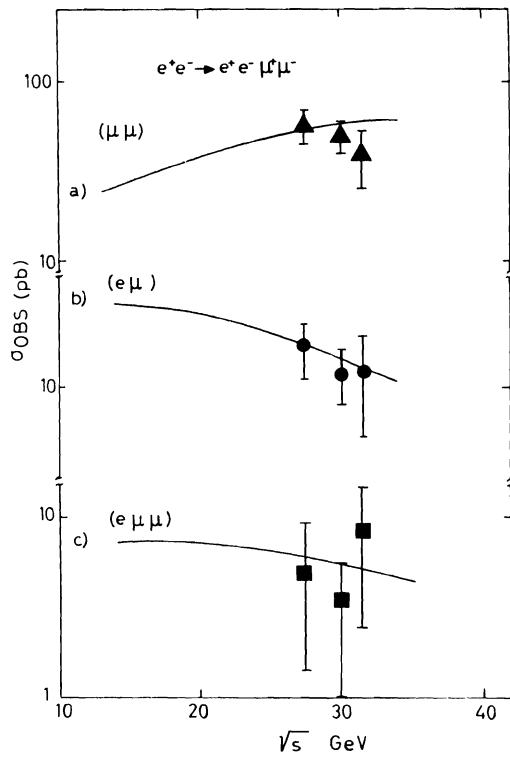


Fig. 7

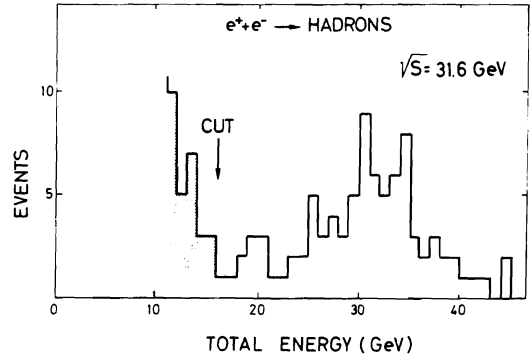
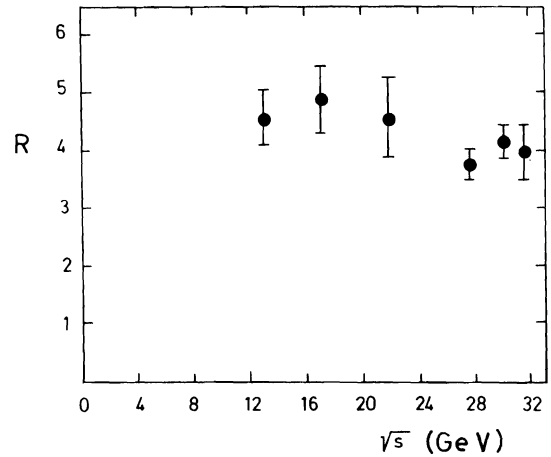


Fig. 9



Statistical error only Shown. Systematic error 15%

Fig. 10

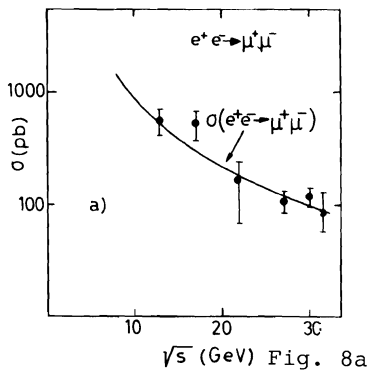


Fig. 8a

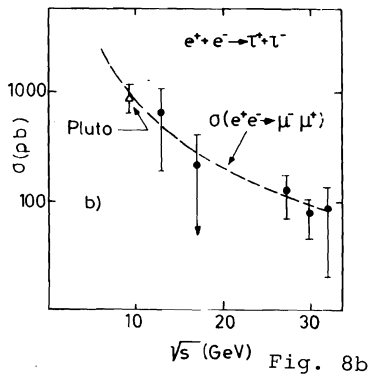
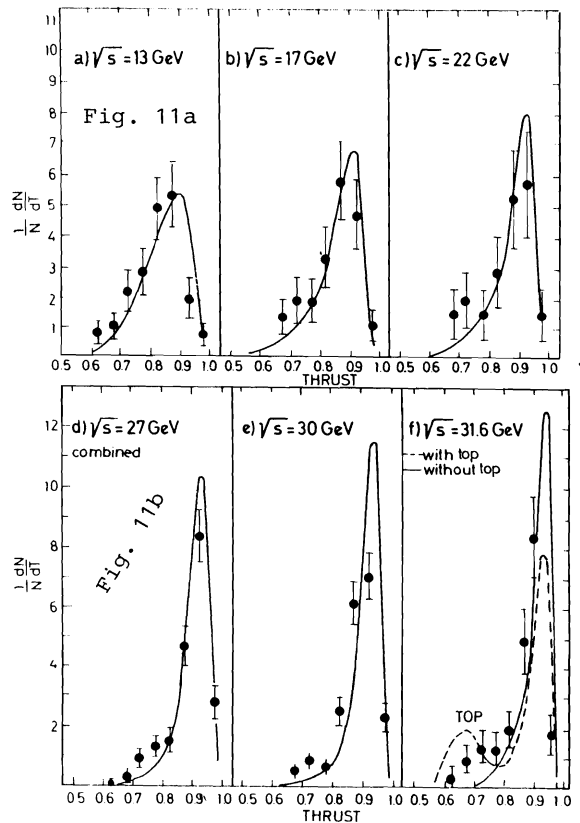


Fig. 8b



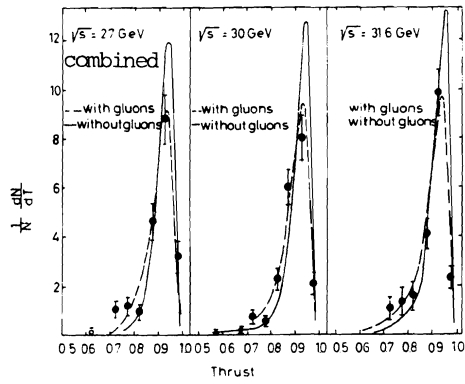


Fig. 11c

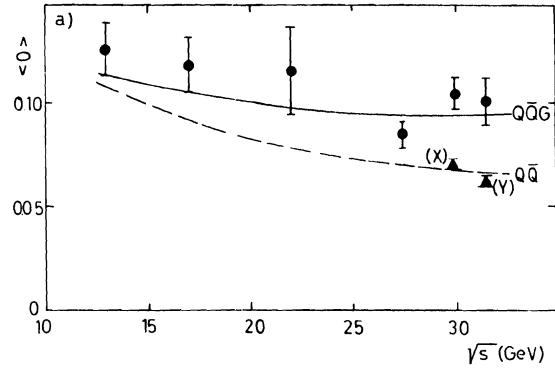


Fig. 13

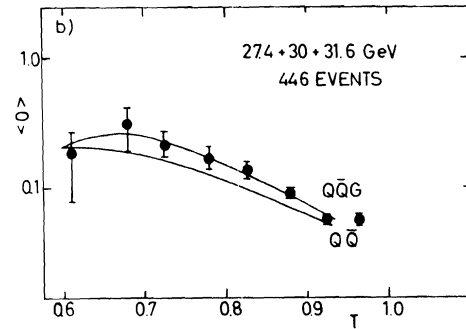


Fig. 14

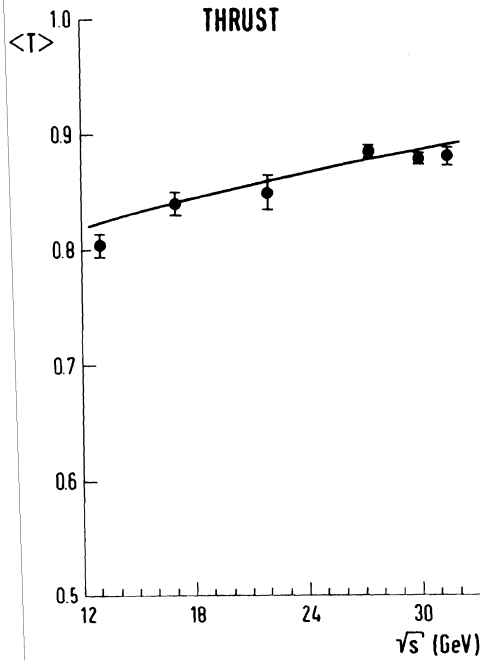


Fig. 12

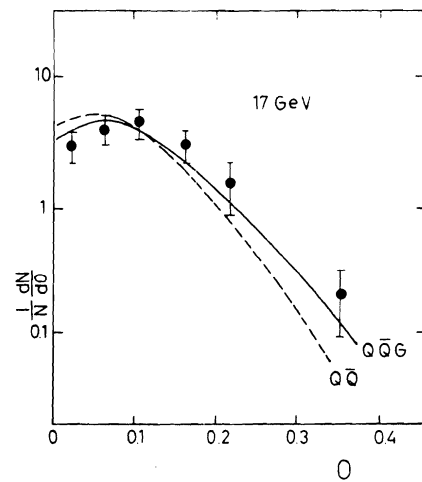


Fig. 15a

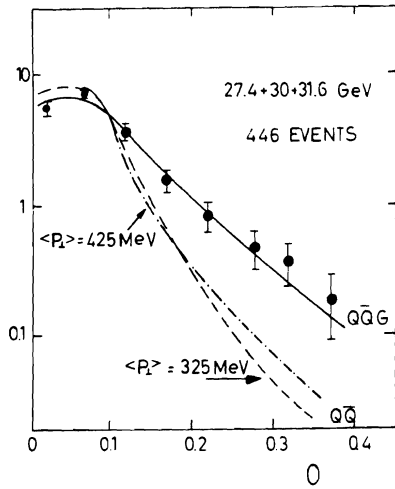


Fig. 15b

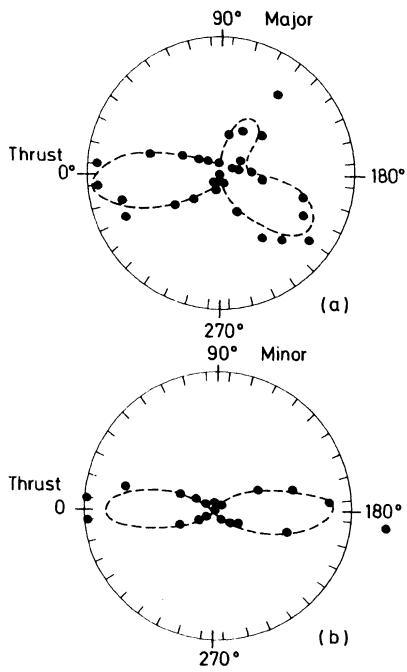


Fig. 16